A Novel Technique to Characterize the Effect of Rain Over a Radome for Radar Applications

Alessio Mancini, *Student, IEEE,* Jorge L. Salazar, *Senior, IEEE,* Rodrigo M. Lebrón, *Student, IEEE,* Boon Leng Cheong

***Abstract*—A novel instrument to characterize the effect of wet radomes in radar systems is presented. The focus of this research is enabling full characterization of radome performance under a variety of conditions including cleanliness, dirtiness, and wetness, and to provide a potential solution for wet radome characterization. The proposed method consists of using a low profile instrument that can be easily integrated into an existing or new radar system. A low profile dielectric antenna connected to the reflectometer employs the time domain gating (TDG) analysis, which is used to minimize the impact of undesirable reflections. The concept was validated with on-field experiments.**

***Index Terms*—radome characterization, time domain gating, reflectometer, dielectric rod antenna**

I. Introduction

In the past, several researchers addressed induced errors in polarimetric parameters of a radar system due to wet radomes. In this paper we highlight some of the important considerations that must be accounted for in order to minimize the impact of wet radomes on the performance of radar systems. For example, the selection of a super-hydrophobic material to coat the external radome skin minimizes the impact of a continuous water film over the surface. This solution significantly improves radar performance when operating at high rain rates. However, it is demonstrated that agents such as pollution and time degradation decrease the radome performance, especially in the presence of water [1], [2]. Blevis in [1], took into account the effect introduced by water on the radome by performing studies in which water was considered as a film. It is not accurate to consider water as a film, since it distributes in droplets or rivulets. Other studies considered the impacts on the radome of artificial rain [2], [4] or natural rain [5], [6]. Salazar in [7] developed an analytical model based on the drop size distribution (DSD) of rainfall to estimate the electrical performance of the wet radome for a dual-polarized phased-array antenna. This study was validated through a numerical simulation and experimental data comparisons. [8] performed a study on the scattering properties of the radome based on its skin surface material, investigating super hydrophobic surfaces, area and inclination of the dome, and rainfall rate. Díaz's study provided additional validation of the drop size distribution model proposed in [7]. Bechini in [9] presented a method for evaluating the attenuation under wet conditions for radars operating at X-band. The correction based on the disdrometer data is complex, because his study is predicated on the assumption that water is a film, and did not account for rivulet effects or wind presence on the exposed side that could produce different attenuation levels on different areas of the radome. A technique based on the Z_{DR} measurement was developed by Gorgucci [10] to perform real-time adjustments on a wet radome. Gorgucci's Z_{DR} calibrations employed two different techniques, sun and weather target calibrations. Results obtained by Gorgucci's two different methods showed only a 0.06 dB difference for the Z_{DR} bias, confirming the validity of his calibration techniques. During a radar campaign in Fortaleza, Schneebeli [3] found that the radome attenuation has a huge impact on measurements. A common technique to characterize radomes is to measure the free-space transmission coefficient. The main inconvenience in using this method is that the perfect probe alignment is difficult to achieve, tests are limited to conformal radomes, the setup is bulky and limits its application to laboratory tests only, and if the sample is too small with respect the antenna beam, the two probes interact.

In this paper a practical solution for improving dual-polarized radar data accuracy is proposed. The solution consists of characterizing, in real time, the effects of the radome caused by imperfections in the fabrication process, by eternal agents such as rain, snow, ice, pollution, or dirt, or by deterioration of the dome over time. This technique is based on the reflection coefficient rather than on the transmission coefficient measurement. By applying time domain gating (TDG) analysis, the effects of unwanted reflections coming from the surrounding environment are reduced. Key components for performing this new technique are: a reflectometer to measure reflections generated at the air-radome interface, the TDG algorithm (implemented in the reflectometer), and a customized dielectric rod antenna employed as a probe. With the technique proposed, it is possible to perform real-time corrections for radome attenuation. The radome is mapped with high-resolution measurements, taking into account the effects introduced by raindrops accumulated on the surface, as well as the scatterer points that are due to imperfections, including those caused by structural joints in the dome. To prove the concept, a laboratory setup was designed to measure the reflections coming from the radome panels. Measurements at X-band for both H- and V-polarization planes have been performed.

II. Concept

The concept, illustrated in Fig. 1a), consists of measuring reflections generated at the air-radome interface, either under

A. Mancini, J. Salazar, R. Lebrón, and B. L. Cheong are with the Department of Electrical and Computer Engineering at the University of Oklahoma, Norman, OK, 73019 USA, see http://www.arrc.ou.edu.

978-1-4673-8823-8/17/$31.00 ©2017 IEEE

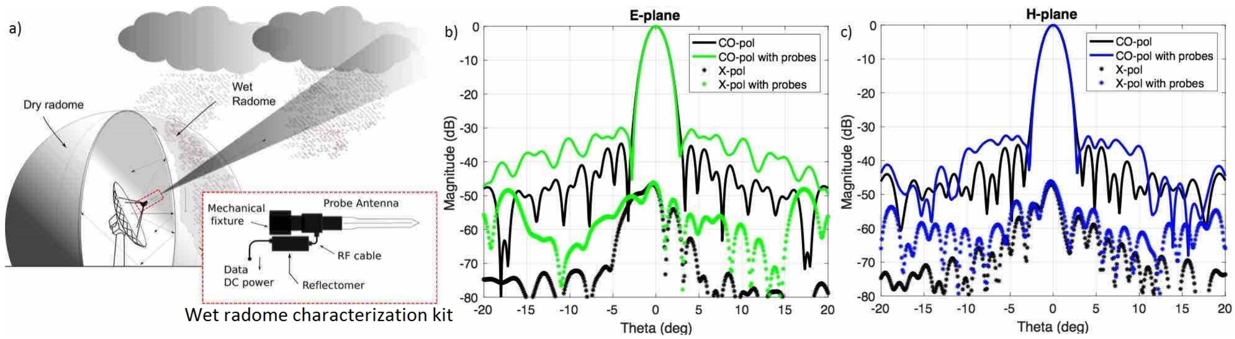

Fig. 1. a) A concept illustration of the proposed radome characterization for the operational radar system. In b) and c) are shown compared simulation results of the radar antenna patterns, with and without the presence of the proposed instrument, for E- and H-plane, respectively.

dry or wet conditions, using a dielectric antenna as a probe. The reflections captured by the probe are read by a single port reflectometer set in time domain. In order to fully characterize the overall surface of the radome, the probe is mounted at the antenna feed position, allowing scanning in azimuth and elevation with resolution dictated by the radar system. To enable measurement of the radome reflections without affecting the dish antenna performance, the size of the proposed system must be smaller than the antenna feed, in order to minimize the attenuation due to blockage. This constraint demands a customized antenna with a small transversal area that enables a narrow beam pattern for high resolution tests. Since the probe is mounted in the radar antenna, it collects reflections generated from the radome in the same direction that the radar is scanning. The test antenna is measuring in its far-field region, in the electromagnetic shadow region of the feed, which is almost not penetrated by the radiation of the radar antenna at the moment of the measurement. Such a method is useful to measure the increased level of reflections due to water on the radome when rain reaches the radar location. To perform the radome characterization, the dielectric antenna is connected to a reflectometer, and the TDG is appropriately set to measure the reflections at the radome interface. Simultaneous measurements of the reflections generated from the radome in the H- and V-planes are possible by using two probes next to each other, where one is 90° rotated with respect to the other one. Another advantage of the customized, low profile antennas is that they will not interfere with radar operations. This is proven through numerical simulations in Ansys HFSS. The influence of the probes on the dish antenna performance, has been evaluated for the dual-polarization, which requires the use of two dielectric rod antennas. Comparative results of the radar antenna with and without the proposed instrument are shown in Fig. 1b) and 1c). Results indicate that the main beam of the reflector system is not affected by the presence of the probes, however a rise of sidelobe level is noticed. This implies the antenna probes require a reduction in size using miniaturization techniques, or that a single dual-polarized antenna should be used. For this prototype, the dielectric antennas employed were not the miniaturized versions that would be necessary for real-time applications. Synchronization between the controlling laptop and the radar is required to trigger the reflectometer to measure when the radar moves to a new position in azimuth or elevation. Synchronization is also necessary to relate the data collected to the actual position. Once the data is collected, through post-processing it is possible to estimate the rain effect on the radome and remove it, improving the radar data quality and eliminating the bias introduced by the wet surface. Under wet conditions, different water formations are possible on various parts of the radome. The presence of rivulets is critical due to their vertical geometry, which induces increases in reflections and attenuation more in the vertical than in the horizontal plane. The traditional system to measure attenuation in a radome is shown in Fig. 2a). In this case, two probes are necessary, one to transmit and the other to receive. The antennas have to be perfectly aligned facing each other, with the sample material located exactly halfway between the probes. Based on this configuration, part of the incident field at the air-radome interface is reflected, and part is transmitted through the sample material. Although this technique provides excellent results, it is impractical for radome characterization in operational radar systems. This procedure, in fact, requires the use of a two-port network analyzer to measure the electric field that is reflected and transmitted through the radome sample. Additional limitations of this technique are the fact that this system is bulky, that it can only characterize samples of flat radomes, and that most of the radomes employed in operational radar systems make use of different shapes (bullet, spherical, conical, etc). In addition, the proposed system is small, lightweight, inexpensive, and easy to implement, allowing installation behind the feed of a dish antenna of current operational systems. The setup employed for this approach is shown in Fig. 2b). To show a preliminary proof of concept, simulations in HFSS were performed considering two different scenarios. The first case used two ports to emulate the system shown in Fig. 2a). A second simulation, to reproduce the scenario in Fig. 2b), used one port and set the second port as an impedance boundary to simulate the free space. Results are presented in Fig. 2c) and 2d). The transmission coefficient for the one port case (Fig. 2d)), is obtained by 1 - R, where R is the reflection coefficient. Simulations show excellent agreement between the two scenarios, and demonstrating that al least for dry radome

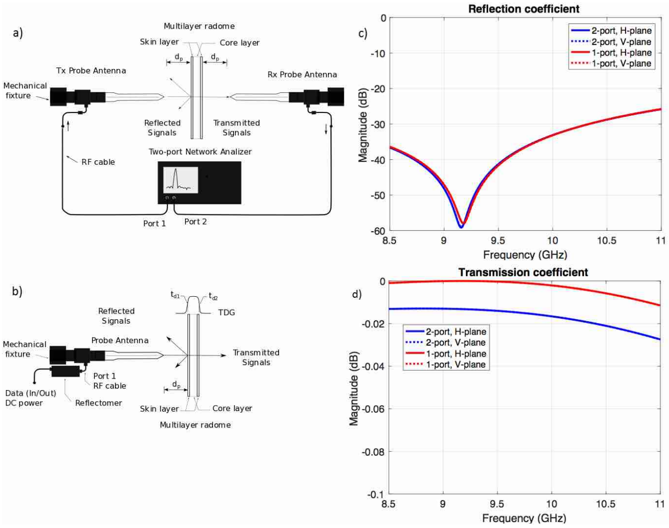

Fig. 2. A schematic representation of the measurement system. a) the conventional method using two probes is shown. b) the new technique using only one probe is shown. HFSS simulations are shown for the reflection (c) and transmission (d) coefficients, for both H- and V-planes.

the absorptions are negligible.

A. *Time domain gating (TDG)*

The concept behind TDG is to use a filter in the time domain. This time filter works exactly the same as a filter in the frequency domain. TDG applications have various uses across disciplines. They have been used in the past to remove discontinuities or reflections in a free-space context, and for tuning purposes [11]. TDG was also used in [12] for radiation pattern measurements, and also for calibration in free-space measurements [13], [14]. TDG was employed in this study to more accurately investigate reflections produced from the source of interest without contamination from the reflections generated by the surrounding environment.

III. Proof of Concept

To validate the concept discussed in the previous section, a laboratory setup was built to enable the testing that provided preliminary results.

A. *Laboratory Setup*

In Fig. 3a) a photograph of the setup is shown. The laboratory setup is composed of five radome panels. The rotary motor with the mounted probe is located in the corner of the setup. The panels are placed abutting each other, however small air gaps between them remain, and they are located at θ = 17, 37, 57, and 77° with respect the initial position of the rotary table. A wooden support was necessary to maintain the radome panels in a stable position above the antenna and to secure the rotary motor as well. The panel-antenna distance is not the same for all tilting angles due to fabrication imperfections of the setup. The radome panel stackup is composed of an inner layer of foam (6.62 mm) and and outer later of teflon (0.53 mm). Metal strips were placed on the top outer part of the radome with the purpose of providing a reference for the measurements.

1) Reflectometer: The novel aspect of this technique is that characterization is based on the reflection coefficient rather than on the transmission coefficient. For this purpose, a vector network analyzer (VNA) reflectometer was used. The VNA works in the frequency range 85 MHz - 14 GHz, and is designed for operation with an external computer which also feeds the device using a USB port. The test port provides the incident signal as the output. To accomplish the reflections measurement, the VNA compares the received (reflected) signal with the source signal.

2) Dielectric rod antenna: To fully characterize the radome and achieve high spatial resolution, an antenna with high gain and narrow beamwidth is necessary. Furthermore, for a mobile station, a low profile antenna probe is also desirable. These requirements are met using a dielectric rod antenna. Such antennas have been employed in [15], [16], and [17]. This antenna consists of a dielectric rod placed in the waveguide aperture. The far-field distance, for a dielectric rod antenna, is 2-3λ (λ = 3.2 cm at 9.4 GHz). In the present research, the radome characterization was performed using a rectangular waveguide and an ABS rod designed to operate at X-band. In Fig. 4a) a photograph of the antenna employed in this study is presented. In Fig. 4b) the electric field level simulated in HFSS is shown. In Fig. 4c) the far-field radiation pattern measured at 9.4 GHz is plotted. The 3 dB-beamwidth is 18°.

3) Radome: The bullet shaped radome of the PX-1000 was employed for the characterization. In Fig. 5, photographs of the radome are shown. This radome has physical external dimensions of 87.23” in diameter, 75.25” in total height, and 31.63” for the height of the cylindrical base. The photo in Fig. 5a) was taken outdoors on a sunny day, so the light coming through the radome is sunlight, and no objects that could project their shadows on the radome were nearby. The panels that compose the radome are made of honeycomb hexagons which have different patterns along the directions of x and y, resulting in the distance between two consecutive hexagons being different in vertical and horizontal directions. Therefore, one would expect that both the distribution of hexagons and the presence of non-homogeneity (dark areas) could affect the level of polarization in the H- and V-planes and their related attenuation. Two panels located next to each other could introduce further attenuation, particularly at the junction. Other issues impacting the attenuation are due to flaws or damage in the radome that are not visible to the eye.

4) Robot: To prove this new concept in a bullet shaped radome, without a radar pedestal, it was necessary to mount the antenna on a device which would allow rotation in azimuth and elevation while keeping the probe orthogonal to the surface of the radome. A six-axis robotic arm (Universal Robots - UR3) was employed to substitute for the radar pedestal. The robot is versatile in that it allows for characterization of radomes with different shapes. With the probe mounted on it, the UR3 has been programmed to perform movements based on spherical coordinates in agreement with the geometry of the radome, and to have a full scan in azimuth and elevation. The robot has been mounted in the position where the radar pedestal of the PX-1000 would sit. In this way, the UR3 was positioned in the geometric center of the cylinder/sphere in order to avoid

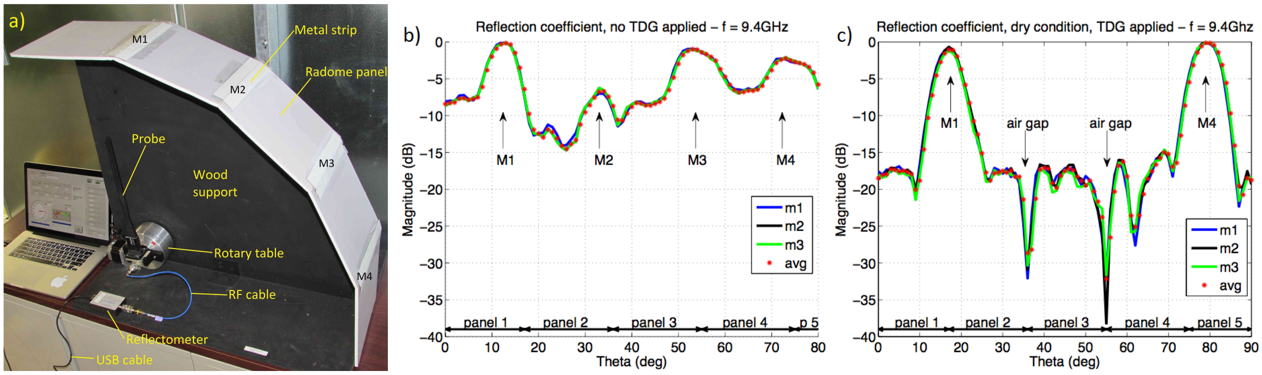

Fig. 3. Shown is the setup employed for the initial measurements: a) a photograph of the setup. b) the results with four metal strips positioned at θ = 17°, 37°, 57°, and 77°, without applying the TDG. c) the results with two metal strips placed at θ = 17° and 77°, with TDG applied. In the plots, "m_1" - "m_3" represents the measurement number, while "avg" is the average of the three measurements.

misalignment during measurements.

B. Preliminary Results

This section is dedicated to describing the experiments performed using the laboratory setup shown in Fig. 3a). The results were obtained at 9.4 GHz. The measurements were performed more than one time and under the same conditions, to assure the reproducibility of the experiment, and to compare the results of each test to the average. The first experiment was performed without applying the TDG. Four metal strips were placed in the air gaps located between the consecutive panels to provide reference in the measurement, as shown in Fig. 3a). The purpose of this experiment was to evaluate if a satisfactory measurement of the reflections could be achieved without using the filter in the time domain. The reflections coming from the metal strips would be expected to be stronger than the ones generated from the rest of the setup, and therefore could be visualized without TDG. In Fig. 3b), the results for this case are shown. When tested, although the metal strips provided high reflection of the signal compared to the ones produced by the radome panels, the multiple paths generated from other generic surfaces of the environment strongly affected the measurements. The second experiment repeated the first, but with applying the TDG. In this test, the strips M2 and M3 were removed, exposing the air gaps between the panels. In Fig. 3c), the results for the second test are shown. Comparing the results from the two scenarios, the necessity of employing the TDG analysis during the measurements is evident.

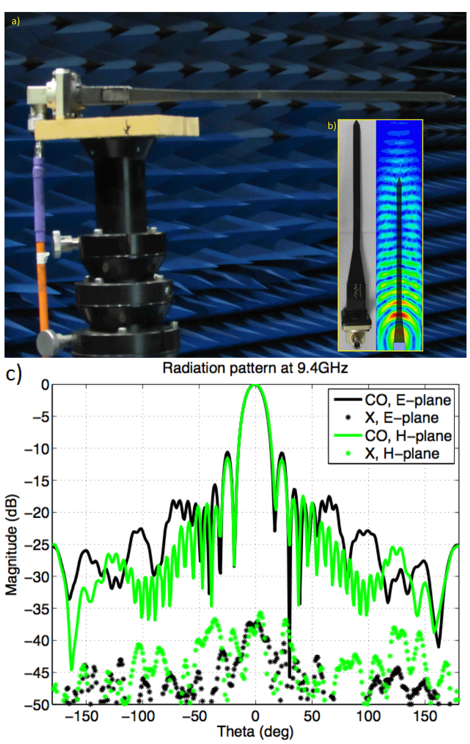

Fig. 4. a) The ABS antenna shown in a photograph taken in the far-field chamber. b) An image of the related electric field simulated in HFSS. c) A plot of the radiation pattern measured in the far-field chamber.

IV. Experimental Results

In this section, the tests performed in the bullet shaped radome (Fig. 5) of the PX-1000 weather radar will be discussed. The tests were executed applying the TDG, for both H- and V-polarizations and considered the radome under dry and wet conditions. The experiment was conducted by measuring one polarization at a time, performing a 360° azimuth scan for each cut in elevation. The range in elevation varied from 0 to 80°. The angle resolutions in azimuth and elevation were 1 and 5° respectively. The dry radome investigation is useful for detection of damages, or non-homogeneous patterns present on the surface that are not necessarily detected by visual inspection. Studies done under wet conditions took place under natural rain. A complication of performing measurements under natural rain conditions is that the full radome characterization, with the mentioned angle resolution, required a long time to be executed (10 mins per azimuth scan). For the measurement to be completed the rain had to last long enough. In the data presented, the storm lasted of sufficient duration to have a full characterization of the radome. However, the rain rate was not constant during the test, which means that scans at different elevation angles might have measured the reflection coefficient under different rain intensities. Also, the rain rate could have changed from the time the test of the first polarization was performed until the time the test of the second

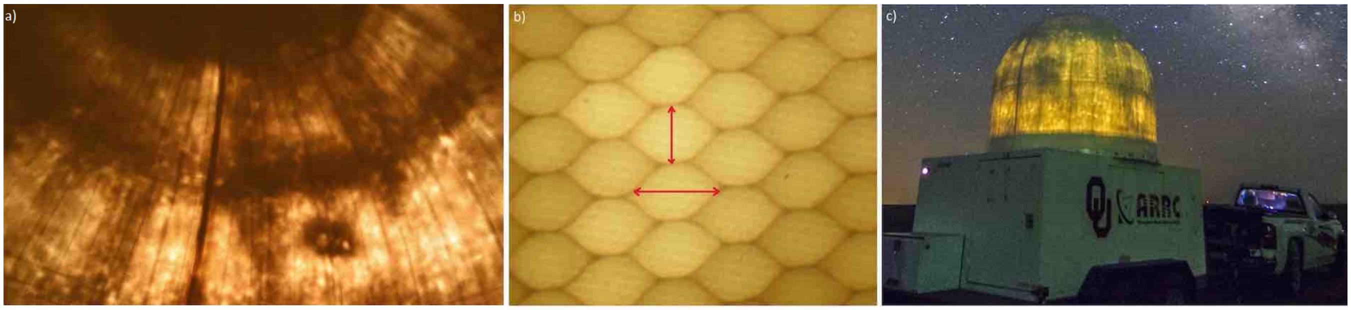

Fig. 5. The PX-1000 radar radome. On the left (a), a close-up of the radome with light penetrating from the exterior. In the center (b), a close-up of the honeycomb core of the dome. On the right (c), a long-exposure photo taken at night (photo courtesy of Jim Kurdzo).

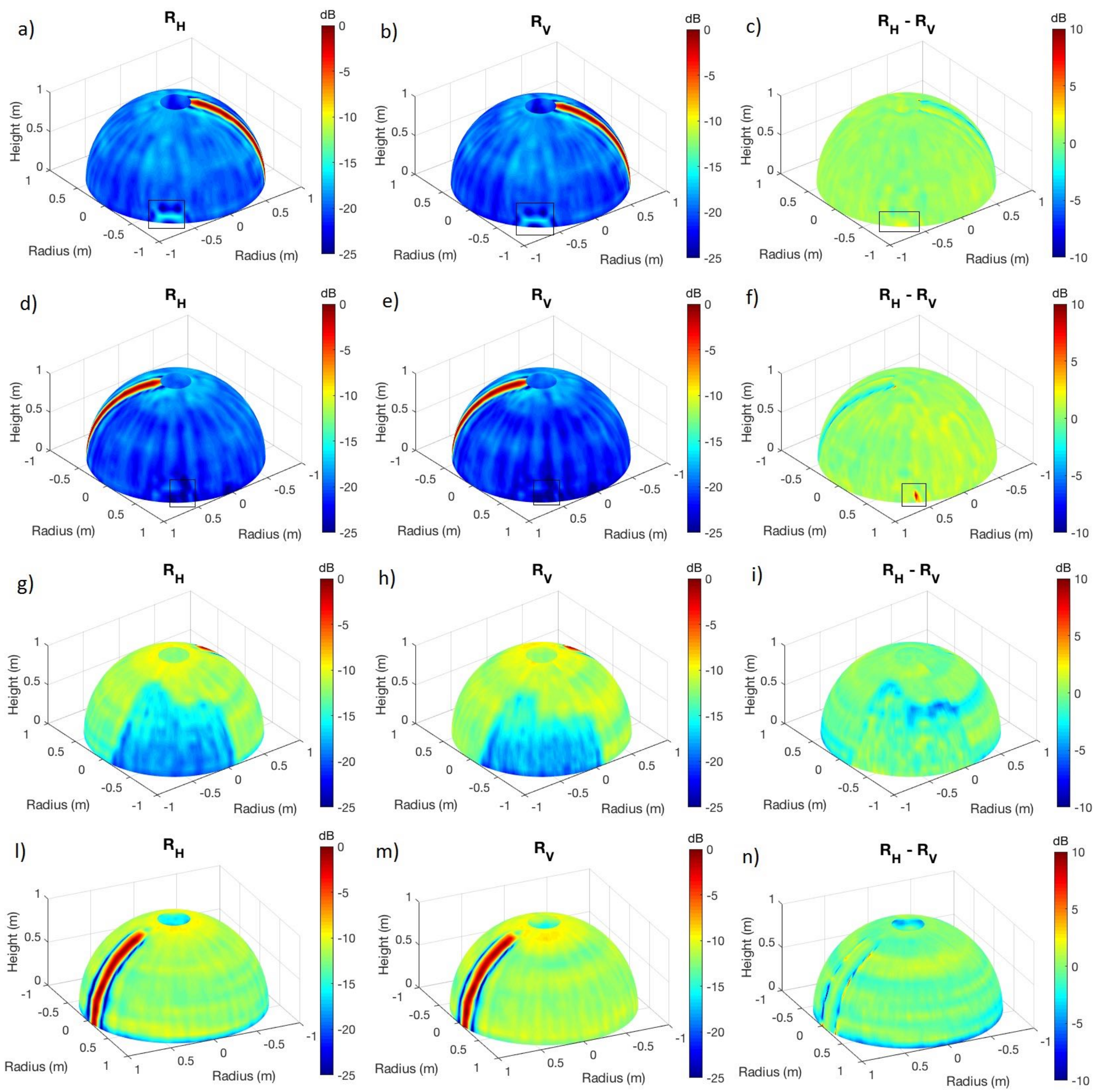

Fig. 6. Shown is the reflection coefficient measurement for the spherical part of the radome under dry conditions, a) to f), and wet conditions g) to n). In order of the columns order are: H-polarization, V-polarization, and the difference between the two polarizations. a), b), c), g), h), and i) show results for one side of the radome. d), e), f), l), m), and n) show results for the opposite side.

polarization was conducted. Before starting the experiments, in a quarter of the radome sphere, Rain-X was applied. Rain-X is a substance to increase the hydrophobic property of surfaces. Rain-X was used only on part of the radome for the purpose of comparing different water distributions on the surface. Water was expected to present as droplets or rivulets on the Rain-X sector, and as a film on the remainder of the radome. It was expected that the two areas would respond differently to the incident signal. The hydrophobic effect due to Rain-X, was thought to potentially have more impact on the H-polarization, since it prevents film formation and keeps water in droplets or rivulets. Results for each of the cases are presented showing the reflection coefficient (R) for H- and V-polarizations, and the difference between the two polarizations: $\mathrm{R_{H,dB}}$ - $\mathrm{R_{V,dB}}$. A vertical metal strip was placed on the outer surface of the radome to provide reference during the tests. The tests were performed at 8.8 GHz.

A. Dry

The results for the spherical part of the radome are shown in Fig. 6a) - f). Looking at Fig. 6a) and 6b), a fabrication imperfection (an air gap on the authors' opinion), not detectable by visual inspection, is noticeable at the base of the sphere, but only present on one side of the radome. The reflections due to this flaw, are generated by diffraction that occurs at the border of the air gap. In Fig. 6c) and 6f), the differential reflection coefficient is shown.

B. Wet

This test was perform on April 17^{th}, 2016, in Norman, Oklahoma. First, the full radome characterization was performed for one polarization, then the test for the other polarization was performed. Results of the rain test are presented in Fig. 6g) - n). The Rain-X effect is highlighted in Fig. 6g) and 6h), in contrast to the other side of the radome shown in Fig. 6l) and 6m). Also, it is noteworthy that at the top of the spherical part of the radome ($\theta \cong 80°$), without any distinction among the different sectors, the level of reflections is higher. At such elevations the component of the gravity force is smaller than at lower elevations, causing the water to stay agglomerated and in bigger drops [7]. The differential reflection coefficient is shown in Fig. 6i) and 6n). A pattern of parallel rings is noticeable, and indicates a stronger difference between the two polarizations. Considering that the rain intensity could have changed during the test, the pattern of parallel rings seems to be consistent and constant in azimuth, therefore it should not be assumed that it is associated with rain rate changes.

V. Conclusion

A novel instrument to characterize real-time dual-polarization performance of a radome was presented. A low profile, customized, narrow beam probe antenna combined with a TDG reflectometer was used for high spatial resolution measurements. Successive experiments were performed on an X-band, bullet shaped radome weather radar (PX-1000). Results under dry conditions individuate non-homogeneous behavior of the radome due to imperfections in the fabrication and assembly processes. Results for wet radome conditions highlighted how various water formations over the radome impact the reflected signals, causing different responses in the two polarizations. The validity of the radome characterization method has been established, and the next step is to design a miniaturized probe to perform measurements in an operative radar.

Acknowledgment

The authors would like to thank Simon Duthoit, Damon Schmidt, and Danny Feland for the help provided.

References

[1] B. Blevis, "Losses due to rain on radomes and antenna reflecting surfaces," *IEEE Trans. Antennas Propag.*, vol. 13, pp. 175–176, 1965.

[2] C. E. Hendrix, J. E. McNally, and R. A. Monzingo, "Depolarization and attenuation effects of radomes at 20 ghz," *IEEE Trans. Antennas Propag.*, vol. 37, pp. 320–328, 1989.

[3] M. Schneebeli, J. Sakuragi, T. Biscaro, C. F. Angelis, I. C. da Costa, C. Morales, L. Baldini, and L. A. T. Machado, "Polarimetric x-band weather radar measurements in the tropics: radome and rain attenuation correction," *Atmos. Meas. Tech.*, vol. 5, pp. 2183–2199, 2012.

[4] M. Kurri and A. Huuskonen, "Measurements of transmission loss of a radome at different rain intensities," *J. Atmos. Oceanic Technol.*, vol. 25, pp. 1590–1599, 2008.

[5] M. Frech, B. Lange, T. Mammen, J. Seltmann, C. Morehead, and J. Rowan, "Influence of a radome on antenna performance," *J. Atmos. Oceanic Technol.*, vol. 30, pp. 313–324, 2013.

[6] S. J. Frasier, F. Kabeche, J. F. I. Ventura, H. Al-Sakka, P. Tabary, J. Beck, and O. Bousquet, "In-place estimation of wet radome attenuation at x band," *J. Atmos. Oceanic Technol.*, vol. 30, pp. 917–928, 2013.

[7] J. L. Salazar-Cerreno, V. Chandrasekar, J. M. Trabal, P. Siquera, R. Medina, E. Knapp, and D. J. McLaughlin, "A Drop Size Distribution (DSD)-Based Model for Evaluating the Performance of Wet Radome for Dual-Polarized Radars," *J. Atmos. Oceanic Technol.*, vol. 31, pp. 2409–2430, 2014.

[8] J. Díaz, J. L. Salazar, A. Mancini, and J. G. Colom, "Radome design and experimental characterization of scattering and propagation properties for atmospheric radar applications." Amer. Meteor. Soc., 2014, pp. 819–823.

[9] R. Bechini, V. Chandrasekar, R. Cremonini, and S. Lim, "Radome attenuation at x-band radar operations," in *Proc. Sixth European Conf. on Radar in Meteorology and Hydrology*. Sibiu, Romania: ERAD 2010, 2010, p. 15.1.

[10] E. Gorgucci, R. Bechini, L. Baldini, R. Cremonini, and V. Chandrasekar, "The influence of antenna radome on weather radar calibration and its real-time assessment," *J. Atmos. Oceanic Technol.*, vol. 30, pp. 676–689, 2012.

[11] B. Archambeault, S. Connor, and J. C. Diepenbrock, "Time domain gating of frequency domain s-parameter data to remove connector end effects for pcb and cable applications," in *2006 IEEE International Symposium on Electromagnetic Compatibility*. IEEE, 2006, pp. 199–202.

[12] G. A. Burrell and A. R. Jamieson, "Antenna radiation pattern measurement using time domain-to-frequency transformation (tft) techniques," in *IEEE Trans. Antennas Propag.* IEEE, 1973, pp. 702–704.

[13] D. K. Ghodgaonkar, V. V. Varadan, and V. K. Varadan, "A free-space method for measurement of dielectric constants and loss tangents at microwave frequencies," *IEEE Trans. Instrum. Meas.*, vol. 38, pp. 789–793, 1989.

[14] M. Zaho, J. D. Shea, S. C. Hagness, and D. W. van der Weide, "Calibrated free-space microwave measurements with an ultrawideband reflectometer-antenna system," *IEEE Microwave and Wireless Components Letters*, vol. 16, pp. 675–677, 2006.

[15] G. E. Mueller and W. A. Tyrrell, "Polyrod antennas," *Alcatel-Lucent Journal*, vol. 26, pp. 837–851, 1947.

[16] R. B. Watson and C. W. Horton, "The radiation pattern of dielectric rods–experiment and theory," *Journal of Applied Physics*, vol. 19, pp. 661–670, 1948.

[17] F. J. Zucker, "Surface-wave antennas," in *Antenna Theory*, R. E. Collin and F. J. Zucker, Eds. McGraw-Hill, 2007, pp. 298–348.

978-1-4673-8823-8/17/$31.00 ©2017 IEEE